Demonstration of a ZnO-Nanowire-Based Nanograting Temperature Sensor

Hongqian CAO, Danran LI, Kanghu ZHOU, and Ye CHEN*

College of Engineering and Applied Sciences, Nanjing University, Nanjing 210093, China

*Corresponding author: Ye CHEN E-mail: yechen@nju.edu.cn

Abstract: In this study, we experimentally demonstrate a miniature fiber thermometer based on tip-integrated ZnO-nanowire-nanograting. The sensor has a diameter less than 1 μm and the length of the Bragg grating is sub-10 μm. The ZnO-nanowire-nanograting is sensitive to the environmental temperature change. Thus, the intensity of the light whose wavelength is in the rising or falling region of the nanograting spectrum will vary with the shift in wavelength due to change in temperature. Taking one wavelength (655 nm) in the rise linear region of the nanograting spectrum, a sensitivity of 0.066 nW/℃ in the air is achieved experimentally. The proposed temperature sensor has the superiorities of compactness, stableness, and easy fabrication compared to regular fiber grating sensors, offering great potential for detecting inside minimal volume environments.

Keywords: Optical-fiber device; ZnO-nanowire; nanograting; temperature sensor

Citation: Hongqian CAO, Danran LI, Kanghu ZHOU, and Ye CHEN, "Demonstration of a ZnO-Nanowire-Based Nanograting Temperature Sensor," *Photonic Sensors*, 2023, 13(1): 230123.

1. Introduction

Optical fiber-based sensors are widely studied. Their advantages of compact size, easy fabrication, low cost, compatibility to fiber system, and immunity to the electromagnetic environment are favored. Many fiber-based sensors have been made in past decades to sense physical and chemical parameters like temperature [1–3], refractive index [4, 5], humidity [6–8], pressure [9, 10], magnetic fields [11, 12], bio/chemical compounds [13, 14] or multi-parameters [15–17]. Standard silica fiber [18–20], photonic crystal fiber [21, 22], and fibers with well-designed structures [23–25] based systems are widely invented. Among them, fiber-grating-based sensors [3, 11, 16, 18, 26–29] are popularly used in engineering applications benefiting from their high sensitivity and stable performance. Conventional fiber gratings are fabricated by phase-mask-assisted ultraviolet (UV) light writing to modulate periodical change of refractive index. However, the weak evanescent field, small index modulation, and large size restrict applications in micro- and nano-environment. With the development of the micro-machining techniques, optical fiber-based micro-devices, for example, taper [26, 27, 30] and nanowire-based [29] sensors fabricated by focused ion beam (FIB) or femtosecond laser methods show a new way. Kou *et al.* [26–28, 30] developed miniaturized Fabry-Perot cavity and nanogratings on optical fiber taper tip for sensing applications. However, due to the limitation of the relatively small refractive index of SiO_2, the length of the grating is longer than 30 μm. As an important representative of one-dimensional wide bandgap semiconductors,

Received: 9 March 2022 / Revised: 9 May 2022

DOI: 10.1007/s13320-022-0663-8
Article type: Regular

ZnO nanowire has been used widely in novel optoelectronic and nanophotonic devices. It is an ideal waveguide due to its high refractive index and compatible coupling with other waveguides. ZnO nanowire shows superiority of much smaller profile compared to optical fiber counterparts. Furthermore, the thermo-optics coefficient of ZnO is one order higher than that of SiO_2 [26, 31], and the variation of refractive of ZnO is higher with the same temperature change. With these advantages, ZnO-nanowire-based gratings have extensive potential applications in micro- and nano-environments.

In this work, a miniaturized ZnO-nanowire-nanograting-based fiber-taper temperature sensor (ZnO-Nanograting sensor) by FIB drilling is proposed and demonstrated experimentally. A less than 10-μm-long grating is milled on a ZnO nanowire with a diameter of about 800 nm. It has periods in 230 nm of 40 periods with a notch in the depth of 100 nm for the first-order resonance. Temperature sensing of the ZnO-Nanograting sensor in the air is demonstrated. Theoretical analysis is conducted as well. The results show that the ZnO-nanograting sensor will have an ideal performance with a precise design and fabrication. The sensor has excellent potential in submicron-size object detection and robust response due to the intriguing properties of flexible design and ultrasmall size.

2. Design and theoretical analysis

In this section, we simulate the reflection spectrums of the ZnO-nanograting sensor with a variation in nanowire diameters, grating length, grove depth, duty cycle, and temperature by analytic calculation. The schematic diagram of the nanograting is shown in Fig. 1. Parameters, d, h, Λ, and δ, represent diameter, grove height, period, and duty cycle of grating, respectively. The basic parameter setting here are: diameter = 0.6 μm, grove depth = 100 nm, period = 190 nm, duty cycle = 50 %, and grating length = 9 μm.

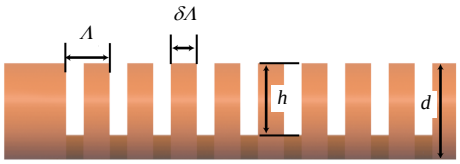

Fig. 1 Schematic diagram of ZnO-nanowire-based nanograting.

The reflection R can be estimated using the expression in [28]:

$$R = \frac{\sinh^2(\sqrt{\kappa^2 - \gamma^2}L)}{\cosh^2(\sqrt{\kappa^2 - \gamma^2}L) - \frac{\gamma^2}{\kappa^2}} \quad (1)$$

where $\kappa = \frac{2\pi L}{\lambda}$, $\gamma = \frac{2\pi}{\lambda}\overline{n_{\text{eff}}} - \frac{\pi}{\Lambda}$, and L are the coupling coefficient, self-coupling coefficient, and grating length, respectively. The reflection is related to the average effective refractive index $\overline{n_{\text{eff}}}$, Bragg period Λ, and length L. Among them, Λ and L are grating processing parameters, and the effective refractive index $\overline{n_{\text{eff}}}$ is accurately calculated by the finite element method considering diameter, duty cycle, and effective grove height of grating. Effective grove height is calculated by (1) [26]. For example, when d = 0.6 μm, δ = 0.5, and h = 100 nm, we get the effective grove height h_{eff} = 62.13 nm by solving (1) [26]. Then $\overline{n_{\text{eff}}}$ = 1.797 is calculated at wavelength 600 nm by utilizing the finite element method (FEM) with ZnO refractive index of nanowire as 1.98. Each wavelength corresponds to a specific effective refractive index $\overline{n_{\text{eff}}}$ in the calculation of (1). The parameters used in the calculation are listed in Table 1.

Table 1 Parameters used in the calculation.

Parameter	Expression and unit	Value
Diameter	d (μm)	0.6 – 1.0
Grating length	L (μm)	5 – 9
Groove depth	h (nm)	100 – 500
Duty cycle	δ (%)	10 – 90
Period	Λ (nm)	190
Effective refractive index	n_{eff}	According to FEM calculation
Temperature	T(℃)	0 – 80

According to the Bragg equation

$$\lambda = 2\overline{n_{\text{eff}}}\Lambda \quad (2)$$

the Bragg wavelength is related to the effective refractive index $\overline{n_{\text{eff}}}$ of ZnO nanowire and Bragg period Λ. In our calculation, we take the period as 190 nm. The results are shown in Fig. 2. It can be found that the thicker diameter, shallower groove depth, and higher duty cycle all conduce higher effective refractive index, inducing a redshift in the Bragg wavelength, which are shown in Figs. 2(a), 2(c), 2(d), and 2(e). Relatively, the variation of the duty cycle has a minor influence on wavelength shift. From Fig. 2(d), the deviation is about 4 nm from 10% to 90% in duty cycle variations, while other parameters change several tens of micrometers. More considerable grating length means longer interaction distance, which impacts the reflection and linewidth of the spectrum rather than resonance wavelength, as shown in Fig. 2(b). The result shows a guideline for designing the nanograting parameters.

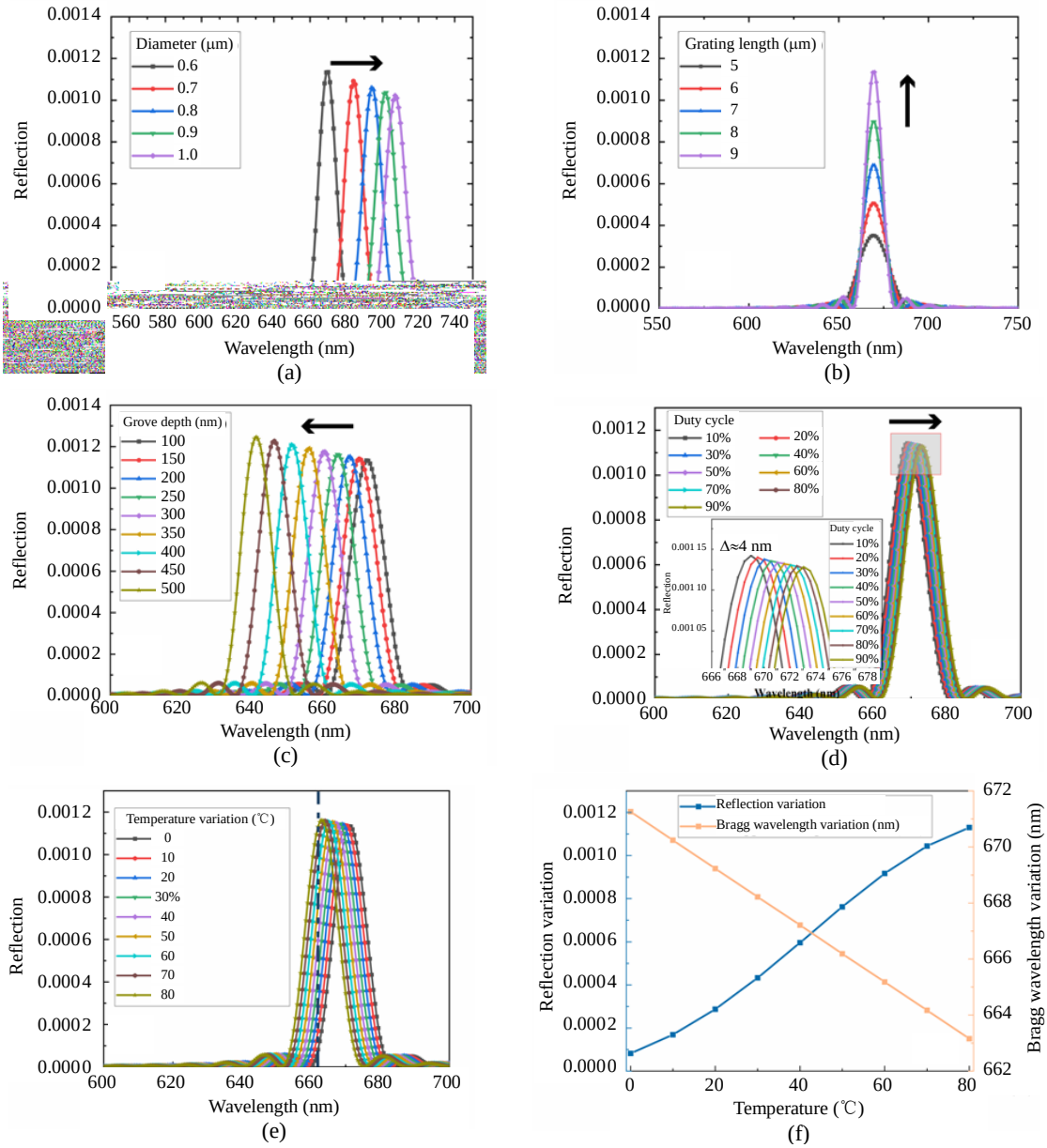

Fig. 2 Bragg wavelength shift of reflection spectrum with variation of (a) diameter, (b) grating length, (c) grove depth, (d) duty cycle, (e) temperature and (f) optical power variation of 661 nm and Bragg wavelength variation of Fig. 1 (e). The basic parameter setting here is diameter = 0.6 μm, grove depth = 100 nm, duty cycle = 50%, and grating length = 9 μm.

The variation of surrounding temperature changes the value of $\overline{n_{\text{eff}}}$. From (2), wavelength change can be written as

$$\Delta\lambda = 2\Delta n_{\text{eff}}\Lambda + 2n_{\text{eff}}\Lambda\Delta T$$
$$= 2\left[\frac{\partial n_{\text{eff}}}{\partial T}\Delta T + (\Delta n_{\text{eff}})_{\text{ep}} + \frac{\partial n_{\text{eff}}}{\partial a}\Delta a\right]\Lambda + 2n_{\text{eff}}\frac{\partial\Lambda}{\partial T}\Delta T \quad (3)$$

where $\frac{\partial n_{\text{eff}}}{\partial T}$ represents the thermo-optics coefficient (TOC) of the refractive index, $(\Delta n_{\text{eff}})_{\text{ep}}$ represents the elasto-optical effect by thermal expansion, $\frac{\partial n_{\text{eff}}}{\partial a}$ represents the change of $\overline{n_{\text{eff}}}$ by diameter change, and $\frac{\partial\Lambda}{\partial T}$ is the thermal expansion coefficient (TEC).

Then, (3) transforms to

$$\frac{\Delta\lambda_B}{\lambda_B\Delta T} = \frac{1}{n_{\text{eff}}}\left[\xi + \frac{(\Delta n_{\text{eff}})_{\text{ep}}}{\Delta T} + \frac{\partial n_{\text{eff}}}{\partial a}\frac{\Delta a}{\Delta T}\right] + \frac{1}{\Lambda}\frac{\partial\Lambda}{\partial T}. \quad (4)$$

Since the elasto-optical effect by thermal expansion and coefficient of thermal expansion of ZnO are invariable and about ppm level [32], respectively, and the value of the thermo-optics coefficient $-2.97\times10^{-4}/℃$ [31] is much larger, then the dominant impact of wavelength shift is due to $\xi\left(=\frac{\partial n_{\text{eff}}}{\partial T}\right)$.

Since ξ is negative [31], according to (4), the wavelength gets a blue shift when the temperature rises, which is shown in Fig. 2(e). Taking one wavelength in the linear region of the spectrum as a work point, *e.g.*, the dashed line at 661 nm in rising edge, the spectrum shift can be measured by a single wavelength laser source. The blue shift of wavelength corresponds to a rise in optical power. The two slopes in Fig. 2(f) show reflection and wavelength variation when the temperature changes. The temperature sensitivity of about −100 pm/℃ near the resonant wavelength of 660 nm is derived. Thus, we can simply demarcate the sensitivity by power change in the measurement. For further accuracy, a fiber grating demodulation method could be used to detect the variation of wavelength and corresponding optical power change. It should be noted that to accommodate the desired measurement range, the wavelength shift should be considered precisely to ensure a linear slope.

3. Fabrication and experiments

The experimental section demonstrates a ZnO-nanograting sensor as a tiny sensor. The fabrication process of tapered optical fiber tip integrated ZnO-Nanograting sensor has three steps [29] [Fig. 3(a)]. Firstly, the tapered optical fiber tip is drawn by a commercial pipette puller (Sutter Instrument Co., MODEL P2000) (Step 1). An adiabatic, smooth profile of fiber taper with a tip diameter of hundreds of nanometers is expected. An optimized profile is beneficial to increase light coupled to ZnO nanowire, achieved by setting CO_2 laser power and pulling velocity. Then, the chemical-vapor-deposition-method-synthesized (CVD) ZnO nanowire is transferred to the tip of a tapered optical fiber tip and bonded with UV glue with the help of two multi-axis translation stages under microscopy (Step 2). Finally, nano gratings are fabricated by FIB (FEI, Helios 600i) milling (Step 3). As mentioned in the theoretical analysis section, the reflected wavelengths of the grating are determined by diameters of ZnO nanowire and grating periods. To get a desired spectrum of nanograting, the effective refractive index is calculated by nanowire diameter, and then the grove period is determined. The finished product's scanning electron microscope (SEM) image is shown in Fig. 3(b). The nanograting has groves of the period Λ=230 nm with 40 periods. The diameter of ZnO in Fig. 3(b) is about 900 nm, which is small.

The experimental setup is shown in Fig. 3(c). The optical characterization of the ZnO-nanograting sensor is performed using an optical spectrum

analyzer (OSA, Ocean Optics) accompanied by a supercontinuum source (YSL SC-5, 500 nm – 700 nm) and a 3 dB (50:50) optical fiber coupler. The supercontinuum source and OSA are connected to the 3 dB ports, while the ZnO-nanograting sensor is connected to the single port. The sensor is stuck on a heat plate and covered with a petri dish to prevent environmental airflow disturbance.

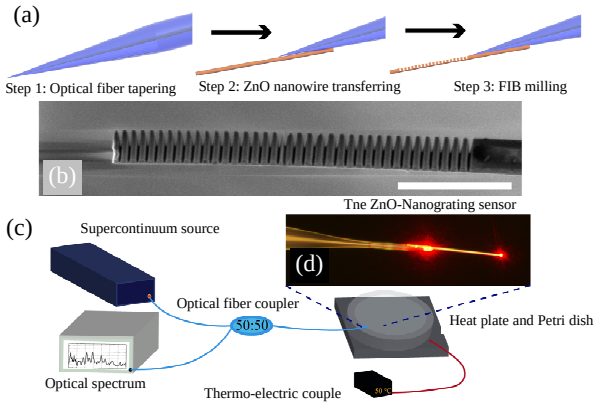

Fig. 3 Schematic diagrams of fabrication process and test of ZnO-nanograting sensor: (a) fabrication process, (b) SEM image (scale bar: 3 μm), (c) schematic for the experiment of ZnO-nanograting sensor, and (d) the microscope image of ZnO-nanograting sensor.

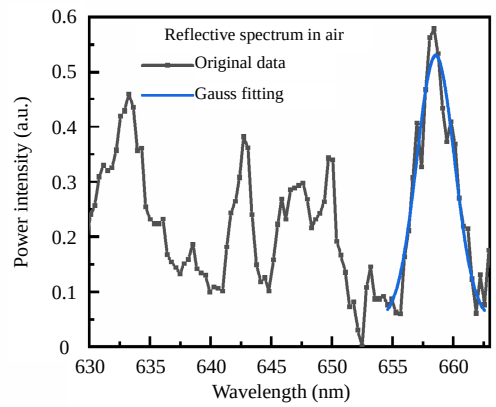

Fig. 4 Multiplex sharp reflection peaks in ZnO-nanograting sensor.

The birefringence of the grating is ignored since it is tiny. From Fig. 4, it can be found that the grating has a multiplex sharp reflection peak; some of them are the higher mode in nanowire while the other miner peaks are interference of reflected light in optical taper and ZnO nanowire. Due to the limited resolution and sensitivity of the visible-light optical spectrum analyzer, the spectrum shown here is not ideal. The wavelength peak around 658 nm fits a Gauss line shape. The wavelength shift could be utilized in temperature sensing with a more precise instrument. A 655-nm-single wavelength laser diode source is used to measure the temperature-optical power relationship.

A thermoelectric couple is used for temperature calibration. Optical power and temperature are recorded synchronously during the hot plate cooling process in Figs. 5(a) and 5(b), respectively. The temperature is set as 80 ℃ at the beginning. It can be seen clearly in Fig. 5 that all the optical power-temperature points get an accurate correspondence, which shows the reliability of the ZnO-nanograting sensor for temperature sensing. The sensitivity is 0.066 nW/℃ and the R^2 parameter is 0.99683.

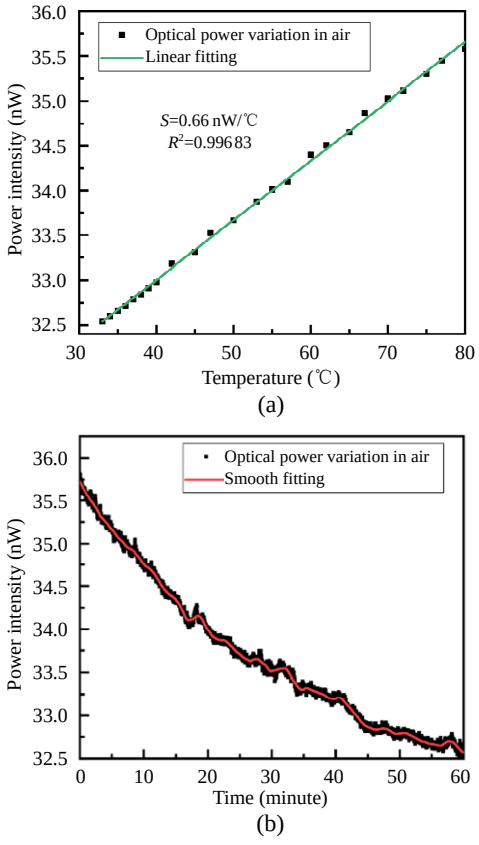

Fig. 5 Optical power variation of ZnO-nanograting sensor (a) with temperature change in the air and (b) over time change.

There are several considerations in this work that should be discussed. Firstly, the device has a deviation of performance with different nanowire

diameters and grating periods, which influences the reflected wavelength and optical spectrum profile. The ideal device could be designed by optimizing these parameters with convenient calculations before microfabrication. Secondly, UV glue's temperature tolerance limitation is −40 ℃ – 140 ℃ so the temperature range we measure in this work is limited. This issue could be solved by using high temperature-resistant glue or direct bonding technology between fiber taper and ZnO nanowire. Thirdly, we only demonstrate a tiny nanograting for temperature sensing application. Application fields could be expanded in other conditions. Last but not least, by precision machining of the FIB milling technology, it is easy to fabricate different kinds of nanograting like tilted gratings, chirped gratings, phase shift gratings. Many other parameters can be measured with this tiny and exquisite platform.

4. Conclusions

In conclusion, we demonstrate an optical fiber tip integrated ZnO-nanowire-nanograting temperature sensor in this work. The sensor has a diameter of less than 1 μm with the first-order Bragg grating with sub-10 μm length. The operating mechanism of the sensor is studied experimentally. The sensitivity of 0.066 nW/℃ in the air is achieved in the experiment. Numerical simulation shows that sensor performance can be optimized by choosing the proper diameter, grating periods, grove depth, and length of the nanograting. The presented miniature sensor has a potential for detecting physical or chemical parameters inside tiny volume environments such as sub-wavelength bubbles, droplets, or bio cells.

Acknowledgment

This study was supported by the National Natural Science Foundation of China (Grants Nos. 62035006 and 62005118).

References

[1] S. J. Qiu, F. Zhou, X. Feng, F. Xu, and Y. Q. Lu, "Lead silicate fiber-based, refractive index-independent temperature sensor," *Journal of Modern Optics*, 2013, 60(10): 851–853.

[2] K. Cao, Y. Liu, and S. Qu, "Compact fiber biocompatible temperature sensor based on a hermetically-sealed liquid-filling structure," *Optics Express*, 2017, 25(24): 29597–29604.

[3] G. Li, L. Ji, G. Li, J. Su, and C. Wu, "High-resolution and large-dynamic-range temperature sensor using fiber Bragg grating Fabry-Perot cavity," *Optics Express*, 2021, 29(12): 18523–18529.

[4] P. Chen, X. Shu, F. Shen, and H. Cao, "Sensitive refractive index sensor based on an assembly-free fiber multi-mode interferometer fabricated by femtosecond laser," *Optics Express*, 2017, 25(24): 29896–29905.

[5] G. An, S. Li, T. Cheng, X. Yan, X. Zhang, X. Zhou, *et al.*, "Ultra-stable D-shaped optical fiber refractive index sensor with graphene-gold deposited platform," *Plasmonics*, 2018, 14(1): 155–163.

[6] X. Li, B. Culshaw, M. Yang, Y. Liao, A. Wang, J. Dai, *et al.*, "Optical fiber humidity sensor with PVDF thin film as sensitive element," *Advanced Sensor Systems and Applications Iv*, 2010, 7853: 705–711.

[7] C. Li, X. Yu, W. Zhou, Y. Cui, J. Liu, and S. Fan, "Ultrafast miniature fiber-tip Fabry-Perot humidity sensor with thin graphene oxide diaphragm," *Optics Letters*, 2018, 43(19): 4719–4722.

[8] N. Wang, H. Zhang, X. Yu, X. Yin, Y. Li, Y. Du, *et al.*, "Optical fiber Fabry-Perot humidity sensor filled with polyvinyl alcohol," *Sensors and Materials*, 2021, 33(3): 105–1062.

[9] X. Li, H. Zhang, C. Qian, Y. Ou, R. Shen, and H. Xiao, "A new type of structure of optical fiber pressure sensor based on polarization modulation," *Optics and Lasers in Engineering*, 2020, 130: 106095.

[10] Y. Zhao, N. Song, F. Gao, X. Xu, J. Liu, and C. Liu, "High-precision photonic crystal fiber-based pressure sensor with low-temperature sensitivity," *Optics Express*, 2021, 29(20): 32453–32463.

[11] J. M. Karanja, Y. Dai, X. Zhou, B. Liu, M. Yang, and J. Dai, "Femtosecond laser ablated FBG multitrenches for magnetic field sensor application," *IEEE Photonics Technology Letters*, 2015, 27(16): 1717–1720.

[12] Z. Liu, H. Cao, and F. Xu, "Fiber-optic Lorentz force magnetometer based on a gold-graphene composite

membrane," *Applied Physics Letters*, 2018, 112(20): 203504.

[13] C. B. Yu, Y. Wu, C. Li, F. Wu, J. H. Zhou, Y. Gong, *et al.*, "Highly sensitive and selective fiber-optic Fabry-Perot volatile organic compounds sensor based on a PMMA film," *Optical Materials Express*, 2017, 7(6): 2111–2116.

[14] S. Hu, G. Yan, C. Wu, and S. He, "An ethanol vapor sensor based on a microfiber with a quantum-dot gel coating," *Sensors (Basel)*, 2019, 19(2): 300.

[15] A. Leal-Junior, A. Frizera, H. Lee, Y. Mizuno, K. Nakamura, T. Paixao, *et al.*, "Strain, temperature, moisture, and transverse force sensing using fused polymer optical fibers," *Optics Express*, 2018, 26(10): 12939–12947.

[16] H. E. Joe, H. Yun, S. H. Jo, M. B. G. Jun, and B. K. Min, "A review on optical fiber sensors for environmental monitoring," *International Journal of Precision Engineering and Manufacturing-Green Technology*, 2018, 5(1): 173–191.

[17] Y. Liang, H. Zhang, H. Guo, W. Lin, and B. Liu, "Simultaneous measurement of temperature and magnetic field based on ionic-liquid-infiltrated side-hole fibers," *Journal of Lightwave Technology*, 2021, 39(21): 7001–7007.

[18] X. Dong, H. Zhang, B. Liu, and Y. Miao, "Tilted fiber Bragg gratings: Principle and sensing applications," *Photonic Sensors*, 2011, 1(1): 6–30.

[19] L. Tong, "Micro/nanofibre optical sensors: challenges and prospects," *Sensors*, 2018, 18(3): 903.

[20] J. H. Chen, D. R. Li, and F. Xu, "Optical microfiber sensors: sensing mechanisms, and recent advances," *Journal of Lightwave Technology*, 2019, 37(11): 2577–2589.

[21] N. A. Mortensen, S. Xiao, and J. Pedersen, "Liquid-infiltrated photonic crystals: enhanced light-matter interactions for lab-on-a-chip applications," *Microfluidics and Nanofluidics*, 2007, 4(1–2): 117–127.

[22] H. Xuan, J. Ju, M. Zhang, W. Jin, and Y. Liao, "In-fiber polarimeters based on hollow-core photonic bandgap fibers," *Optics Express*, 2009, 17(15): 13246–51324.

[23] J. Ma, J. Ju, L. Jin, and W. Jin, "A compact fiber-tip micro-cavity sensor for high-pressure measurement," *IEEE Photonics Technology Letters*, 2011, 23(21): 1561–1563.

[24] B. L. Li, D. R. Li, J. H. Chen, Z. Y. Liu, G. H. Wang, X. P. Zhang, *et al.*, "Hollow core micro-fiber for optical wave guiding and microfluidic manipulation," *Sensors and Actuators B: Chemical*, 2018, 262: 953–957.

[25] A. D. Gomes, M. Becker, J. Dellith, M. I. Zibaii, H. Latifi, M. Rothhardt, *et al.*, "Multimode Fabry-Perot interferometer probe based on vernier effect for enhanced temperature sensing," *Sensors (Basel)*, 2019, 19(3): 453.

[26] J. L. Kou, S. J. Qiu, F. Xu, and Y. Q. Lu, "Demonstration of a compact temperature sensor based on first-order Bragg grating in a tapered fiber probe," *Optics Express*, 2011, 19(19): 18452–18457.

[27] J. Kou, S. Qiu, F. Xu, Y. Lu, Y. Yuan, and G. Zhao, "Miniaturized metal-dielectric-hybrid fiber tip grating for refractive index sensing," *IEEE Photonics Technology Letters*, 2011, 23(22): 1712–1714.

[28] J. L. Kou, M. Ding, J. Feng, Y. Q. Lu, F. Xu, and G. Brambilla, "Microfiber-based Bragg gratings for sensing applications: a review," *Sensors (Basel)*, 2012, 12(7): 8861–8876.

[29] D. Li, N. Wang, T. Zhang, G. Wu, Y. Xiong, Q. Du, *et al.*, "Label-free fiber nanograting sensor for real-time in situ early monitoring of cellular apoptosis," *Advanced Photonics*, 2022, 4(1): 016001.

[30] J. L. Kou, J. Feng, L. Ye, F. Xu, and Y. Q. Lu, "Miniaturized fiber taper reflective interferometer for high temperature measurement,''*Optics Express*, 2010, 18(13): 14245–14250.

[31] T. A. Dar, A. Agrawal, P. K. Sen, R. J. Choudhary, and P. Sen, "Thermo-optic coefficients of pure and Ni doped ZnO thin films," *Thin Solid Films*, 2016, 603: 115–118.

[32] H. M. O'bryan, L. G. Uitert, E. D. Kolb, and G. Zydzik, "Thermal expansion of ZnO," *Journal of the American Ceramic Society*, 1978, 61: 269.